Optimal Precoding for Orthogonalized Spatial Multiplexing in Closed-Loop MIMO Systems

Young-Tae Kim, Heunchul Lee, Seokhwan Park, and Inkyu Lee

***Abstract*—In this paper, we propose a new precoding algorithm for orthogonalized spatial multiplexing (OSM) systems over flat-fading multiple-input multiple-output (MIMO) channels. The OSM scheme was recently introduced for closed-loop MIMO systems which allows single symbol decodable maximum likelihood detection. To further improve the performance of the OSM system, we propose a new precoding method by maximizing the minimum Euclidean distance between constellation points in the effective channel. In order to efficiently identify the parameters of a precoder which maximizes the minimum distance, we introduce a partitioning approach. Through analysis, it is shown that one real value parameter and two bits are required for feedback information for precoding in 16-QAM systems. Simulation results demonstrate that our algorithm provides 9dB and 7.5dB gains at a bit error rate (BER) of 10^{-4} over the conventional OSM systems for 4-QAM and 16-QAM, respectively. We also confirm that the performance of the proposed scheme is the same as that of the optimum closed-loop MIMO systems in terms of the minimum distance. Consequently, our precoding algorithm significantly improves the system performance with a small increase of feedback amount.**

***Index Terms*—Closed-loop MIMO system, precoding design, ML receiver, limited feedback, minimum Euclidean distance**

I. Introduction

COMMUNICATION over multiple-input multiple-output (MIMO) channels has been the subject of intense research over the past several years. MIMO channels can offer much greater diversity advantages and higher spatial multiplexing (SM) gains over their single-input single-output (SISO) counterpart [1][2][3]. Normally, two approaches have been considered to exploit such aspects of MIMO channels. One is space time coding directed towards maximizing diversity gain [4][5][6], and the other is the SM which focuses on increasing channel throughput [7][8][9].

When the communication environment is slowly time varying, we can assume that channel state information (CSI) is available at the transmitter via feedback in frequency division duplex (FDD) systems or via the reciprocal principle in time division duplex (TDD) systems. Many studies on such closed-loop MIMO systems have been based on singular value decomposition (SVD) of the channel transfer matrix [10][11][12]. For practical applications, a transmitter with limited feedback information has been studied to utilize system resources more efficiently [13][14]. These works focus on maximizing mutual information, minimizing uncoded error rate or minimizing some functions of the mean squared error (MSE) matrix. Linear receivers are employed in [11][12][13] which result worse performance than maximum likelihood (ML) receivers. To approach the optimal performance of systems with ML receivers in terms of uncoded error rate, the minimum Euclidean distance between constellation points in the effective channel must be maximized [13]. However, deriving a closed-form solution to maximize the minimum distance is quite difficult and the decoding complexity of ML receivers may become prohibitive in MIMO systems.

Recently, orthogonalized spatial multiplexing (OSM) has been proposed which achieves orthogonality between transmitted symbols by applying phase rotation at the transmitter [15][16]. The OSM scheme is a new closed-loop MIMO system which does not rely on the SVD. By applying rotation operations to the transmitted symbols, the OSM system allows a simple ML decoder at the receiver. Also, for the OSM system, only one phase feedback value is required for the transmitter. Thus, compared to conventional SVD-based transmission methods, the OSM scheme exhibits a good system performance gain with lower complexity and feedback overhead. One salient feature of the OSM scheme is that the transmitted data symbols experience the same channel quality. This may lead to an incorrect conclusion that additional precoding would not improve the OSM performance. However, this is not the case since each of the inphase/quadrature components of the transmitted symbol still has different channel gains.

Recognizing this situation, we introduce new precoding schemes for OSM systems which further improve the performance. First, we consider a criterion based on the minimum Euclidean distance, since the minimum Euclidean distance accounts for the symbol error probability. To efficiently identify the parameters of the proposed precoder which maximizes the minimum distance, we introduce a partitioning approach. Our derivation indicates that one real value parameter and one bit (two bits) are required for feedback information for the proposed precoder in 4-QAM (16-QAM) systems. Also, we propose two other suboptimum precodings for our schemes to reduce the feedback information. Power loading for the OSM proposed in [17] can be considered as a special case of the proposed precoder.

The simulation results show that our optimal precoding obtains 9dB and 7.5dB gains over the conventional OSM case at a bit error rate (BER) of 10^{-4} for 4-QAM and 16-QAM, respectively. Also we compare our proposed solution with the optimal system in [18] in terms of the minimum distance. We verify that the proposed system equipped with symbol

Manuscript received October 26 2007; revised April 17, 2008. This research was supported in part by the Ministry of Knowledge Economy, Korea, under the Information Technology Research Center support program supervised by the Institute for Information Technology Advancement (IITA-2008-C1090-0801-0013) and in part by grant No. R01-2006-000-11112-0 from the Basic Research Program of the Korea Science and Engineering Foundation. This paper was presented in part at IEEE International Conference on Communications, Beijing, China, May 2008.

The authors are with the School of Electrical Engineering, Korea University, Seoul 136-701, Korea (e-mail: reftm@korea.ac.kr, {heunchul, shpark}@wireless.korea.ac.kr and inkyu@korea.ac.kr).

Digital Object Identifier 10.1109/JSAC.2008.081021.

0733-8716/08/$25.00 © 2008 IEEE

Authorized licensed use limited to: IEEE Xplore. Downloaded on October 16, 2008 at 20:47 from IEEE Xplore. Restrictions apply.

by symbol detection achieves the performance identical to the optimal system in [18] based on joint ML detection with lower complexity.

The remainder of this paper is organized as follows: In Section II, we present the system model and review the OSM system. In Section III, we propose new precoding algorithms for enhancing the performance of OSM systems. Also, we introduce a partitioning approach for identifying the precoder parameters. In Section IV, we describe simulation results to demonstrate the optimality of our precoding algorithms. Finally, we conclude in Section V.

II. System Descriptions

In this section, we consider a SM system with M_t transmit and M_r receive antennas in a frequency flat fading channel. Throughout this paper, normal letters represent scalar quantities, boldface letters indicate vectors and boldface uppercase letters designate matrices. With a bar accounting for complex variables, for any complex notation $\overline{c}$, we denote the real and imaginary part of $\overline{c}$ by $\Re[\overline{c}]$ and $\Im[\overline{c}]$, respectively.

We consider the complex channel output as

$$\overline{\mathbf{y}} = \overline{\mathbf{H}}\overline{\mathbf{x}} + \overline{\mathbf{n}} \tag{1}$$

where $\overline{\mathbf{x}} \in \mathbb{C}^{M_t \times 1}$ is the complex transmitted signal, $\overline{\mathbf{y}} \in \mathbb{C}^{M_r \times 1}$ indicates the complex received signal, $\overline{\mathbf{H}} \in \mathbb{C}^{M_r \times M_t}$ represents the complex channel matrix with the (i,j)th element $\overline{h}_{ij}$ denoting the fading coefficient between the jth transmit and the ith receive antenna, and $\overline{\mathbf{n}} \sim \mathcal{N}(0, \sigma_n^2 \mathbf{I}_{M_r})$ stands for circularly symmetric complex Gaussian noise. Here, $\mathbf{I}_{M_r}$ denotes an identity matrix of size M_r. Each channel realization is assumed to be known at the receiver.

In what follows, we give a brief review of the OSM scheme [15][16]. The transmitter structure diagram of the OSM is given in [15]. The OSM orthogonalizes a channel by applying a rotation operation at the transmitter and transmits two independent data streams. Then, a single symbol decodable ML detection is employed at the receiver which greatly decreases the detection complexity. To simplify the presentation, we focus on $M_t = 2$. In [15], a method of extending the original OSM scheme to systems with $M_t \geq 2$ was introduced.

To orthogonalize the channel, the OSM adopts the following transformation as

$$\mathcal{F}(\overline{\mathbf{x}}, \theta) = \begin{bmatrix} 1 & 0 \\ 0 & \exp(j\theta) \end{bmatrix} \mathbf{s}(\overline{\mathbf{x}})$$

where θ is the rotation phase angle applied to the second antenna and $\mathbf{s}(\overline{\mathbf{x}})$ is defined as

$$\mathbf{s}(\overline{\mathbf{x}}) \triangleq \begin{bmatrix} s_1(\overline{\mathbf{x}}) \\ s_2(\overline{\mathbf{x}}) \end{bmatrix} = \begin{bmatrix} \Re[\overline{x}_1] + j\Re[\overline{x}_2] \\ \Im[\overline{x}_1] + j\Im[\overline{x}_2] \end{bmatrix}.$$

Employing the above transformation, equation (1) can be rewritten as

$$\overline{\mathbf{y}} = \overline{\mathbf{H}}\mathcal{F}(\overline{\mathbf{x}}, \theta) + \overline{\mathbf{n}} = \overline{\mathbf{H}}_\theta \mathbf{s}(\overline{\mathbf{x}}) + \overline{\mathbf{n}} \tag{2}$$

where $\overline{\mathbf{H}}_\theta$ accounts for the effective channel matrix for $\mathbf{s}(\overline{\mathbf{x}})$, represented by

$$\overline{\mathbf{H}}_\theta = \overline{\mathbf{H}} \begin{bmatrix} 1 & 0 \\ 0 & \exp(j\theta) \end{bmatrix}.$$

Equivalently, the real-valued representation of the system (2) is given as [15] [16]

$$\begin{aligned} \mathbf{y} &= \begin{bmatrix} \Re[\overline{\mathbf{y}}] \\ \Im[\overline{\mathbf{y}}] \end{bmatrix} = \mathbf{H}_\theta \mathbf{s}(\mathbf{x}) + \mathbf{n} \\ &= \begin{bmatrix} \Re[\overline{\mathbf{H}}_\theta] & -\Im[\overline{\mathbf{H}}_\theta] \\ \Im[\overline{\mathbf{H}}_\theta] & \Re[\overline{\mathbf{H}}_\theta] \end{bmatrix} \begin{bmatrix} \Re[\mathbf{s}(\overline{\mathbf{x}})] \\ \Im[\mathbf{s}(\overline{\mathbf{x}})] \end{bmatrix} + \begin{bmatrix} \Re[\overline{\mathbf{n}}] \\ \Im[\overline{\mathbf{n}}] \end{bmatrix} \\ &= \begin{bmatrix} \mathbf{h}_1^\theta \ \mathbf{h}_2^\theta \ \mathbf{h}_3^\theta \ \mathbf{h}_4^\theta \end{bmatrix} \mathbf{s}(\mathbf{x}) + \mathbf{n} \end{aligned} \tag{3}$$

where the real column vector $\mathbf{h}_i^\theta$ of length $2M_r$ denotes the ith column of the effective real-valued channel matrix $\mathbf{H}_\theta$, $\mathbf{s}(\mathbf{x})$ represents $[\ \Re[\overline{x}_1]\ \Im[\overline{x}_1]\ \Re[\overline{x}_2]\ \Im[\overline{x}_2]\ ]^t$ and $\mathbf{n}$ indicates $[\ \Re[\overline{\mathbf{n}}^t]\ \Im[\overline{\mathbf{n}}^t]\ ]^t$.

From the real-valued representation of the channel matrix in (3), it is easy to see that the column vectors $\mathbf{h}_1^\theta$ and $\mathbf{h}_2^\theta$ are orthogonal to $\mathbf{h}_3^\theta$ and $\mathbf{h}_4^\theta$, respectively ($\mathbf{h}_1^\theta \perp \mathbf{h}_3^\theta$ and $\mathbf{h}_2^\theta \perp \mathbf{h}_4^\theta$), regardless of θ. We also notice that we have $\mathbf{h}_1^\theta \cdot \mathbf{h}_4^\theta = -\mathbf{h}_2^\theta \cdot \mathbf{h}_3^\theta$ for all θ, where $\mathbf{a} \cdot \mathbf{b}$ denotes the inner (dot) product between vectors $\mathbf{a}$ and $\mathbf{b}$. In this case, $\mathbf{H}_\theta$ becomes orthogonal if and only if $\mathbf{h}_1^\theta \perp \mathbf{h}_4^\theta$ and $\mathbf{h}_2^\theta \perp \mathbf{h}_3^\theta$ ($\mathbf{h}_1^\theta \cdot \mathbf{h}_4^\theta = -\mathbf{h}_2^\theta \cdot \mathbf{h}_3^\theta = 0$).

Denoting the rotation angle $\theta = \theta_o$ for the orthogonality between $\mathbf{h}_1^\theta$ and $\mathbf{h}_4^\theta$ (or $\mathbf{h}_2^\theta$ and $\mathbf{h}_3^\theta$), we obtain θ_o as [15] [16]

$$\theta_o = \tan^{-1}\left(\frac{B}{A}\right) \pm \frac{\pi}{2}$$

where $A = \sum_{m=1}^{M_r} |\overline{h}_{m1}||\overline{h}_{m2}| \sin\left(\angle\overline{h}_{m2} - \angle\overline{h}_{m1}\right)$ and $B = \sum_{m=1}^{M_r} |\overline{h}_{m1}||\overline{h}_{m2}| \cos\left(\angle\overline{h}_{m2} - \angle\overline{h}_{m1}\right)$. This rotation angle makes $\mathbf{h}_1^{\theta_o}$ and $\mathbf{h}_2^{\theta_o}$ (or $\mathbf{h}_3^{\theta_o}$ and $\mathbf{h}_4^{\theta_o}$) orthogonal to each other.

Utilizing this orthogonality, the ML estimate of transmitted symbols $\hat{\overline{x}}_1$ and $\hat{\overline{x}}_2$ can be obtained as [15] [16]

$$\hat{\overline{x}}_1 = \arg\min_{\overline{x}_1 \in Q} \left|\left| \mathbf{y} - \begin{bmatrix} \mathbf{h}_1^{\theta_o} \ \mathbf{h}_2^{\theta_o} \end{bmatrix} \begin{bmatrix} \Re[\overline{x}_1] \\ \Im[\overline{x}_1] \end{bmatrix} \right|\right|^2 \tag{4}$$

and

$$\hat{\overline{x}}_2 = \arg\min_{\overline{x}_2 \in Q} \left|\left| \mathbf{y} - \begin{bmatrix} \mathbf{h}_3^{\theta_o} \ \mathbf{h}_4^{\theta_o} \end{bmatrix} \begin{bmatrix} \Re[\overline{x}_2] \\ \Im[\overline{x}_2] \end{bmatrix} \right|\right|^2 \tag{5}$$

where Q is a signal constellation of size M_c. As a result, the complexity of the ML detection of the OSM reduces from $O(M_c^2)$ to $O(M_c)$. Thus, compared to SVD-based transmission schemes, the OSM achieves lower complexity and feedback overhead [15] [16].

III. Precoding Schemes for OSM

First we discuss the necessity of precoding for OSM systems. We can see from equations (4) and (5) that a solution for the OSM system is transformed into two SISO equations. Here, $\mathbf{h}_1^{\theta_o}$, $\mathbf{h}_2^{\theta_o}$, $\mathbf{h}_3^{\theta_o}$ and $\mathbf{h}_4^{\theta_o}$ represent the channel column vectors corresponding to the inphase/quadrature components of two transmitted symbols. It was shown in [15] and [16] that the subspace spanned by $\mathbf{h}_1^{\theta_o}$ and $\mathbf{h}_2^{\theta_o}$ is orthogonal to that spanned by $\mathbf{h}_3^{\theta_o}$ and $\mathbf{h}_4^{\theta_o}$ in the OSM system. Also, it is easy to see that we have $||\mathbf{h}_1^{\theta_o}|| = ||\mathbf{h}_3^{\theta_o}||$, $||\mathbf{h}_2^{\theta_o}|| = ||\mathbf{h}_4^{\theta_o}||$, and $\mathbf{h}_1^{\theta_o} \cdot \mathbf{h}_2^{\theta_o} = \mathbf{h}_3^{\theta_o} \cdot \mathbf{h}_4^{\theta_o}$. Because of this fact, one may think that a precoding operation is not necessary for an OSM system. However, we can note that the column vectors $\mathbf{h}_1^{\theta_o}$ and $\mathbf{h}_3^{\theta_o}$ are not orthogonal to $\mathbf{h}_2^{\theta_o}$ and $\mathbf{h}_4^{\theta_o}$, respectively. Also, $||\mathbf{h}_1^{\theta_o}|| = ||\mathbf{h}_3^{\theta_o}||$ is not equal to $||\mathbf{h}_2^{\theta_o}|| = ||\mathbf{h}_4^{\theta_o}||$. As a result, the channel energies corresponding to the inphase

Authorized licensed use limited to: IEEE Xplore. Downloaded on October 16, 2008 at 20:47 from IEEE Xplore. Restrictions apply.

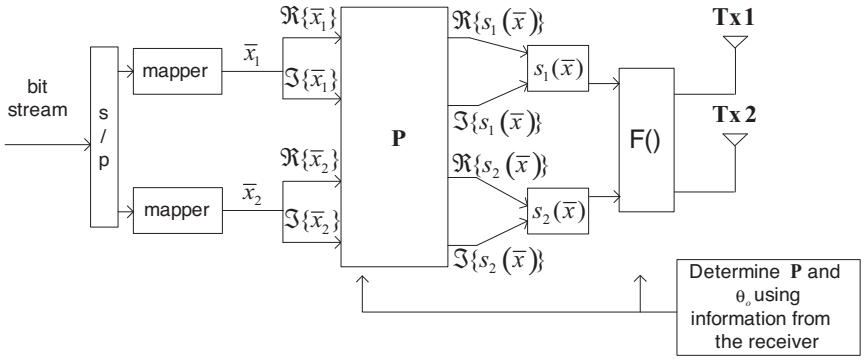

Fig. 1. Schematic diagram of the transmitter structure for the proposed scheme

and quadrature components are still different and the symbol with a smaller channel gain can degrade the performance.

Motivated by this observation, we present a new precoding algorithm for OSM systems which maximizes the minimum distance, denoted by d_{min}, since the performance of the optimum ML receiver depends on the minimum Euclidean distance in the received signal constellation [19]. In general, deriving a closed-form solution which maximizes d_{min} is difficult, since the number of candidates for d_{min} grows exponentially depending on the number of antennas and modulation levels used. However, since the OSM systems orthogonalize the channel associated with the transmitted symbols, the structure of OSM makes the process of d_{min} maximization easier. In this section, we first introduce the optimal precoding for an OSM system. Then, we will present two other suboptimal precoding algorithms for OSM systems which are special cases of the proposed precoding. Again, to simplify the presentation, we assume $M_t = 2$.

To construct the precoding for OSM systems, we can rewrite the system model in (3) as

$$\mathbf{y} = \mathbf{H}_{\theta_o}\mathbf{P}\mathbf{s}(\mathbf{x}) + \mathbf{n} \tag{6}$$

where $\mathbf{P}$ denotes the 4-by-4 real precoding matrix. Then, in order to preserve orthogonality between the transmitted symbols, we can choose $\mathbf{P}$ as a block orthogonal matrix,

$$\mathbf{P} = \begin{bmatrix} \mathbf{P}_1 & \mathbf{0} \\ \mathbf{0} & \mathbf{P}_2 \end{bmatrix} \tag{7}$$

where $\mathbf{P}_1$ and $\mathbf{P}_2$ are 2-by-2 real matrices. Here, $\mathbf{P}_1$ and $\mathbf{P}_2$ control the channel gains associated with $\overline{x}_1$ and $\overline{x}_2$, respectively. Since the channel qualities of $\mathbf{h}_1^\theta$ and $\mathbf{h}_2^\theta$ are identical to those of $\mathbf{h}_3^\theta$ and $\mathbf{h}_4^\theta$ in terms of d_{min}, $\mathbf{P}_1$ and $\mathbf{P}_2$ in the precoding matrix in (7) can be set to be the same ($\mathbf{P}_1 = \mathbf{P}_2$). Thus, our precoder design problem reduces to identifying a 2-by-2 real matrix $\mathbf{P}_1$.

In choosing $\mathbf{P}_1$, there may be many different methods. In this paper, we decompose $\mathbf{P}_1$ into three 2-by-2 real matrices to simplify the derivation. Consider the SVD of a matrix $\mathbf{A}$ as $\mathbf{A} = \mathbf{U}\Lambda\mathbf{V}^*$, where $\mathbf{U}$, $\mathbf{V}$ and Λ are the left and right singular value decomposition matrices and the singular value matrix, respectively. In the case where $\mathbf{A}$ is a 2-by-2 real matrix, $\mathbf{U}$ and $\mathbf{V}$ can be represented by rotation matrices. Based on this observation, we propose a new precoding matrix $\mathbf{P}$ in (7) where $\mathbf{P}_1 = \mathbf{P}_2$ is decomposed into the same matrix structure as the SVD. Then, the precoding matrix can be defined as

$$\mathbf{P} = \mathbf{R}'_{\theta 1}\mathbf{D}'\mathbf{R}'_{\theta 2} = \begin{bmatrix} \mathbf{R}_{\theta 1} & 0 \\ 0 & \mathbf{R}_{\theta 1} \end{bmatrix}\begin{bmatrix} \mathbf{D} & 0 \\ 0 & \mathbf{D} \end{bmatrix}\begin{bmatrix} \mathbf{R}_{\theta 2} & 0 \\ 0 & \mathbf{R}_{\theta 2} \end{bmatrix} \tag{8}$$

where

$$\mathbf{R}_{\theta 1} = \begin{bmatrix} \cos\theta_1 & -\sin\theta_1 \\ \sin\theta_1 & \cos\theta_1 \end{bmatrix}, \quad \mathbf{D} = \begin{bmatrix} p & 0 \\ 0 & \sqrt{2-p^2} \end{bmatrix}$$

$$\text{and} \quad \mathbf{R}_{\theta 2} = \begin{bmatrix} \cos\theta_2 & -\sin\theta_2 \\ \sin\theta_2 & \cos\theta_2 \end{bmatrix}.$$

By substituting the precoding matrix (8) into the system model in (6), we have

$$\begin{aligned} \mathbf{y} &= \mathbf{H}_{\theta_o}\mathbf{R}'_{\theta 1}\mathbf{D}'\mathbf{R}'_{\theta 2}\mathbf{s}(\mathbf{x}) + \mathbf{n} \\ &= \mathbf{H}_R^\theta\mathbf{D}'\mathbf{R}'_{\theta 2}\mathbf{s}(\mathbf{x}) + \mathbf{n} \\ &= \mathbf{H}_p^\theta\mathbf{s}(\mathbf{x}) + \mathbf{n} \end{aligned}$$

where $\mathbf{H}_R^\theta \triangleq \mathbf{H}_{\theta_o}\mathbf{R}'_{\theta 1} = [\mathbf{h}_{1R}^\theta\ \mathbf{h}_{2R}^\theta\ \mathbf{h}_{3R}^\theta\ \mathbf{h}_{4R}^\theta]$ and $\mathbf{H}_p^\theta \triangleq \mathbf{H}_{\theta_o}\mathbf{R}'_{\theta 1}\mathbf{D}'\mathbf{R}'_{\theta 2} = [\mathbf{h}_{1p}^\theta\ \mathbf{h}_{2p}^\theta\ \mathbf{h}_{3p}^\theta\ \mathbf{h}_{4p}^\theta]$. We assume that the total transmit power is constrained to be $\mathbf{E}\{\mathrm{tr}(\mathbf{P}\mathbf{s}(\mathbf{x})\mathbf{s}(\mathbf{x})^T\mathbf{P}^T)\} = P_T$ which equals $\mathbf{E}\{\mathrm{tr}(\mathbf{s}(\mathbf{x})\mathbf{s}(\mathbf{x})^T)\} = P_T$. The structure of the proposed precoding system is shown in Fig. 1.

Now, by transforming Equation (4) into the equation with the precoding (8), the ML solution for $\overline{x}_1$ in our scheme can be rewritten as

$$\hat{\overline{x}}_1 = \arg\min_{\overline{x}_1 \in Q} \left\| \mathbf{y} - [\ \mathbf{h}_{1p}^\theta\ \mathbf{h}_{2p}^\theta\ ] \begin{bmatrix} \Re[\overline{x}_1] \\ \Im[\overline{x}_1] \end{bmatrix} \right\|^2. \tag{9}$$

Similarly, $\overline{x}_2$ can be estimated by using $\mathbf{h}_{3p}^\theta$ and $\mathbf{h}_{4p}^\theta$. Since the channel gains of $\overline{x}_1$ and $\overline{x}_2$ are the same in terms of d_{min}, we will consider only one ML solution (9) from now on.

To obtain the precoding matrix which maximizes d_{min}, we need to compute three parameters θ_1, θ_2 and p for (8). Because it is very complex to jointly optimize these three parameters, we simplify the computation by prefixing θ_1 with the inner rotation value introduced in [20]. Even though this approach may not be optimal for OSM systems, we will confirm through simulations that the proposed precoding achieves the performance identical to that of the optimum closed-loop MIMO systems in [18].

The orthogonality between $\mathbf{h}_{1R}^\theta$ and $\mathbf{h}_{2R}^\theta$ is achieved if the inner product of $\mathbf{h}_{1R}^\theta$ and $\mathbf{h}_{2R}^\theta$ becomes zero as [20]

$$\begin{aligned} (\mathbf{h}_{1R}^\theta)^T\mathbf{h}_{2R}^\theta = &\left(||\mathbf{h}_2^{\theta_o}||^2 - ||\mathbf{h}_1^{\theta_o}||^2\right)\cos\theta_1\sin\theta_1 \\ &+(\cos^2\theta_1 - \sin^2\theta_1)(\mathbf{h}_1^{\theta_o})^T\mathbf{h}_2^{\theta_o} = 0. \end{aligned} \tag{10}$$

Authorized licensed use limited to: IEEE Xplore. Downloaded on October 16, 2008 at 20:47 from IEEE Xplore. Restrictions apply.

Solving Equation (10) with respect to θ_1 yields the following rotation angle

$$\theta_1 = \tan^{-1}\left(\frac{C \pm \sqrt{C^2+4D^2}}{2D}\right) \tag{11}$$

where $C = ||\mathbf{h}_2^{\theta_o}||^2 - ||\mathbf{h}_1^{\theta_o}||^2$ and $D = (\mathbf{h}_1^{\theta_o})^T\mathbf{h}_2^{\theta_o}$. Here, $||\mathbf{h}_{1R}^{\theta}||$ is maximized for $\theta_1 = \tan^{-1}\left(\frac{C+\sqrt{C^2+4D^2}}{2D}\right)$, whereas $||\mathbf{h}_{2R}^{\theta}||$ is maximized for $\theta_1 = \tan^{-1}\left(\frac{C-\sqrt{C^2+4D^2}}{2D}\right)$. Because both of two solutions make the same d_{min}, we consider only the first case ($||\mathbf{h}_{1R}^{\theta}|| \geq ||\mathbf{h}_{2R}^{\theta}||$). Note that the magnitudes of $\mathbf{h}_{1R}^{\theta}$ and $\mathbf{h}_{2R}^{\theta}$ equal the first and the second singular values of the matrix $\mathbf{H}$, respectively [20].

Now that θ_1 is computed in (11), the other two parameters θ_2 and p need to be determined. In what follows, we will show that our scheme requires only a finite set of p and θ_2 for feedback information. Thus, just a few bits are sufficient for indicating the chosen set of p and θ_2. In this work, we identify the optimal parameters p_{opt} and θ_{2opt} with the following criterion

$$(p_{opt},\ \theta_{2opt}) = \arg \max_{0\leq p\leq\sqrt{2},\ \ 0\leq\theta_2\leq\pi/4} d_{min}(p,\theta_2) \tag{12}$$

where $d_{min}(p,\theta_2)$ represents the minimum distance as a function of p and θ_2. We limit the search area of θ_2 to $0 \leq \theta_2 \leq \pi/4$ in Equation (12), because d_{min} in $\pi/4 \leq \theta_2 \leq 2\pi$ is symmetric to that in $0 \leq \theta_2 \leq \pi/4$. Since the max-min function in Equation (12) is nonlinear, it is a difficult problem to find a closed form solution. To simplify this problem, we introduce a partitioning approach which separates the search area in terms of p and θ_2. Note that the optimal precoding parameters p_{opt} and θ_{2opt} in (12) are dependent on modulation levels. In the following, we will present the optimized parameters for 4-QAM and 16-QAM constellations based on the partitioning approach.

A. Optimal precoding for 4-QAM and 16-QAM

To identify p_{opt} and θ_{2opt}, we should find the maximum value of d_{min} for the $p-\theta_2$ region. From the results derived in Appendix A and B, the optimum solutions can be obtained as

4-QAM :

$$\begin{cases} p_{opt} = \sqrt{6/(k+3)}, & \theta_{2opt} = \pi/4 \\ d_{min}^2 = 4k||\mathbf{h}_{2R}^{\theta}||^2/(k+3) & \text{if } \ 1 \leq k < 7 \\ p_{opt} = \sqrt{2}, & \theta_{2opt} = 0.464 \\ d_{min}^2 = 2k||\mathbf{h}_{2R}^{\theta}||^2/5 & \text{if } \ k > 7 \end{cases} \tag{13}$$

16-QAM :

$$\begin{cases} p_{opt} = \sqrt{6/(k+3)}, & \theta_{2opt} = \pi/4 \\ d_{min}^2 = 4k||\mathbf{h}_{2R}^{\theta}||^2/(k+3) & \text{if } \ 1 \leq k < 7.59 \\ p_{opt} = \sqrt{42/(k+21)}, & \theta_{2opt} = 0.489 \\ d_{min}^2 = 10.8k||\mathbf{h}_{2R}^{\theta}||^2/(k+21) & \text{if } \ 7.59 \leq k < 43.1 \\ p_{opt} = \sqrt{182/(k+91)}, & \theta_{2opt} = 0.345 \\ d_{min}^2 = 22.6k||\mathbf{h}_{2R}^{\theta}||^2/(k+91) & \text{if } \ 43.1 \leq k < 101 \\ p_{opt} = \sqrt{2}, & \theta_{2opt} = 0.245 \\ d_{min}^2 = 2k||\mathbf{h}_{2R}^{\theta}||^2/17 & \text{if } \ k > 101 \end{cases} \tag{14}$$

where k is defined as $||\mathbf{h}_{1R}^{\theta}||^2/||\mathbf{h}_{2R}^{\theta}||^2$. Note that there are only two or four distinct cases for representing the optimum precoder parameters θ_2 and p, and that each case can be determined by a single variable k.

TABLE I
CLOSED FORM EXPRESSIONS OF p_{opt} AND θ_{2opt} FOR THE PROPOSED PRECODING

Mod	Case	p_{opt}	θ_{2opt}
4-QAM	$1 \leq k < 7$	1	$\pi/4$
	$k \geq 7$	$\sqrt{2}$	0.464
16-QAM	$1 \leq k < 7.59$	1	$\pi/4$
	$7.59 \leq k < 43.1$	1	0.488
	$43.1 \leq k < 101$	1	0.345
	$k \geq 101$	$\sqrt{2}$	0.245

It is clear that the partitioning approach presented in Appendix A and B is effective for identifying the maximum of d_{min}. We note that the boundary of the partition is critical. Also, $||\mathbf{h}_{2p}^{\theta}|| = ||\mathbf{h}_{1p}^{\theta} + n\mathbf{h}_{2p}^{\theta}||$ for $n = 1, 2, ..., \log_2 M - 1$ in M-QAM systems is an important equation to determine the maximum of d_{min}. The approach made in this section can be extended to higher modulation systems such as 64-QAM. It is expected that θ_2 and p can be expressed as 3 bits in 64-QAM.

In the proposed precoding systems, two real values θ_1 and k are needed for feedback in addition to θ_o which is required in the original OSM. For solutions (13) and (14), k should be reported to the transmitter to compute p_{opt} and θ_{2opt}. We can simplify the representation to reduce feedback information without a performance loss. We first recognize that the variation in p_{opt} is small in Equations (13) and (14) in terms of k. Thus, we can simply replace the variable p with 1 or $\sqrt{2}$, and the final result for p and θ_2 is depicted in Table I. Note that the case $p = 1$ indicates no power loading in (8) ($\mathbf{D} = \mathbf{I}$). Also, the precoder with $p = \sqrt{2}$ means that the smaller channel gain in $\mathbf{H}_R^{\theta}$ is not utilized as can be seen in (8). With this simplification, instead of feeding back the value k to the transmitter, only one bit and two bits are required for feedback information in 4-QAM and 16-QAM systems, respectively. In the simulation section, it will be shown that this simplification causes no performance loss compared to the optimum case.

B. Suboptimum precoding for OSM

As the proposed precoder consists of three different matrices in (8), we may reduce the complexity of the precoding process by employing only a subset of matrices in (8) at the expense of a little performance loss. First, when the diagonal matrix $\mathbf{D}$ in (8) is neglected, the precoding matrix in Equation (8) becomes

$$\begin{aligned} \mathbf{R}_{\theta 1}\mathbf{R}_{\theta 2} &= \begin{bmatrix} \cos(\theta_1+\theta_2) & -\sin(\theta_1+\theta_2) \\ \sin(\theta_1+\theta_2) & \cos(\theta_1+\theta_2) \end{bmatrix} \\ &= \begin{bmatrix} \cos\theta_r & -\sin\theta_r \\ \sin\theta_r & \cos\theta_r \end{bmatrix} \end{aligned} \tag{15}$$

where $\theta_r = \theta_1 + \theta_2$. Then, the new precoding matrix $\mathbf{R}_{\theta 1}\mathbf{R}_{\theta 2}$ can be represented by a single parameter θ_r. Here, θ_r is determined by $\theta_r = \theta_1 + \arg\max_{\theta_2} d_{min}(\theta_2)$, where θ_1 is computed in (11) and $d_{min}(\theta_2)$ denotes the minimum distance as a function of θ_2 in the above precoding system. This will be referred to as "OSM with rotation precoding", and the result is listed in Table II. The detailed derivation in Table II is omitted for simplification of the presentation.

Another simplification is made possible by considering only the diagonal matrix $\mathbf{D}$ in (8). This can be viewed as

Authorized licensed use limited to: IEEE Xplore. Downloaded on October 16, 2008 at 20:47 from IEEE Xplore. Restrictions apply.

TABLE II
CLOSED FORM EXPRESSIONS OF θ_r FOR OSM WITH ROTATION PRECODING

Mod	Case	θ_r	
4-QAM	$1 \le k < 3$	$\pi/4$	
	$k \ge 3$	α	$A=5\|\|\mathbf{h}_{1R}^{\theta}\|\|^4-10\|\|\mathbf{h}_{1R}^{\theta}\|\|^2\|\|\mathbf{h}_{2R}^{\theta}\|\|^2+5\|\|\mathbf{h}_{2R}^{\theta}\|\|^4$ $B=5\|\|\mathbf{h}_{1R}^{\theta}\|\|^2\|\|\mathbf{h}_{2R}^{\theta}\|\|^2-2\|\|\mathbf{h}_{1R}^{\theta}\|\|^4-3\|\|\mathbf{h}_{2R}^{\theta}\|\|^4$ $C=\|\|\mathbf{h}_{2R}^{\theta}\|\|^4$
16-QAM	$1 \le k < 3$	$\pi/4$	
	$3 \le k < 19.5$	α	$A=5\|\|\mathbf{h}_{1R}^{\theta}\|\|^4-10\|\|\mathbf{h}_{1R}^{\theta}\|\|^2\|\|\mathbf{h}_{2R}^{\theta}\|\|^2+5\|\|\mathbf{h}_{2R}^{\theta}\|\|^4$ $B=5\|\|\mathbf{h}_{1R}^{\theta}\|\|^2\|\|\mathbf{h}_{2R}^{\theta}\|\|^2-2\|\|\mathbf{h}_{1R}^{\theta}\|\|^4-3\|\|\mathbf{h}_{2R}^{\theta}\|\|^4$ $C=\|\|\mathbf{h}_{2R}^{\theta}\|\|^4$
	$19.5 \le k < 43.6$ $110 \le k < 132$	β	$A=13\|\|\mathbf{h}_{1R}^{\theta}\|\|^4-26\|\|\mathbf{h}_{1R}^{\theta}\|\|^2\|\|\mathbf{h}_{2R}^{\theta}\|\|^2+13\|\|\mathbf{h}_{2R}^{\theta}\|\|^4$ $B=13\|\|\mathbf{h}_{1R}^{\theta}\|\|^2\|\|\mathbf{h}_{2R}^{\theta}\|\|^2-11\|\|\mathbf{h}_{1R}^{\theta}\|\|^4-2\|\|\mathbf{h}_{2R}^{\theta}\|\|^4$ $C=9\|\|\mathbf{h}_{1R}^{\theta}\|\|^4$
	$43.6 \le k < 83$	α	$A=20\|\|\mathbf{h}_{1R}^{\theta}\|\|^4-40\|\|\mathbf{h}_{1R}^{\theta}\|\|^2\|\|\mathbf{h}_{2R}^{\theta}\|\|^2+20\|\|\mathbf{h}_{2R}^{\theta}\|\|^4$ $B=20\|\|\mathbf{h}_{1R}^{\theta}\|\|^2\|\|\mathbf{h}_{2R}^{\theta}\|\|^2-14\|\|\mathbf{h}_{1R}^{\theta}\|\|^4-6\|\|\mathbf{h}_{2R}^{\theta}\|\|^4$ $C=9\|\|\mathbf{h}_{1R}^{\theta}\|\|^4+6\|\|\mathbf{h}_{1R}^{\theta}\|\|^2\|\|\mathbf{h}_{2R}^{\theta}\|\|^2+\|\|\mathbf{h}_{2R}^{\theta}\|\|^4$
	$83 \le k < 110$	β	$A=29\|\|\mathbf{h}_{1R}^{\theta}\|\|^4-58\|\|\mathbf{h}_{1R}^{\theta}\|\|^2\|\|\mathbf{h}_{2R}^{\theta}\|\|^2+29\|\|\mathbf{h}_{2R}^{\theta}\|\|^4$ $B=29\|\|\mathbf{h}_{1R}^{\theta}\|\|^2\|\|\mathbf{h}_{2R}^{\theta}\|\|^2-27\|\|\mathbf{h}_{1R}^{\theta}\|\|^4-2\|\|\mathbf{h}_{2R}^{\theta}\|\|^4$ $C=25\|\|\mathbf{h}_{1R}^{\theta}\|\|^4$
	$132 \le k < 190$	α	$A=68\|\|\mathbf{h}_{1R}^{\theta}\|\|^4-136\|\|\mathbf{h}_{1R}^{\theta}\|\|^2\|\|\mathbf{h}_{2R}^{\theta}\|\|^2+68\|\|\mathbf{h}_{2R}^{\theta}\|\|^4$ $B=68\|\|\mathbf{h}_{1R}^{\theta}\|\|^2\|\|\mathbf{h}_{2R}^{\theta}\|\|^2-42\|\|\mathbf{h}_{1R}^{\theta}\|\|^4-26\|\|\mathbf{h}_{2R}^{\theta}\|\|^4$ $C=25\|\|\mathbf{h}_{1R}^{\theta}\|\|^4+30\|\|\mathbf{h}_{1R}^{\theta}\|\|^2\|\|\mathbf{h}_{2R}^{\theta}\|\|^2+9\|\|\mathbf{h}_{2R}^{\theta}\|\|^4$
	$k \ge 190$	α	$A=85\|\|\mathbf{h}_{1R}^{\theta}\|\|^4-170\|\|\mathbf{h}_{1R}^{\theta}\|\|^2\|\|\mathbf{h}_{2R}^{\theta}\|\|^2+85\|\|\mathbf{h}_{2R}^{\theta}\|\|^4$ $B=85\|\|\mathbf{h}_{1R}^{\theta}\|\|^2\|\|\mathbf{h}_{2R}^{\theta}\|\|^2-74\|\|\mathbf{h}_{1R}^{\theta}\|\|^4-11\|\|\mathbf{h}_{2R}^{\theta}\|\|^4$ $C=64\|\|\mathbf{h}_{1R}^{\theta}\|\|^4+16\|\|\mathbf{h}_{1R}^{\theta}\|\|^2\|\|\mathbf{h}_{2R}^{\theta}\|\|^2+\|\|\mathbf{h}_{2R}^{\theta}\|\|^4$
$\alpha = \cos^{-1}\sqrt{\frac{-B+\sqrt{B^2-AC}}{A}}$, $\beta = \cos^{-1}\sqrt{\frac{-B-\sqrt{B^2-AC}}{A}}$			

TABLE III
CLOSED FORM EXPRESSIONS OF p_{power} FOR OSM WITH POWER LOADING ($||\mathbf{h}_1^{\theta}|| \le ||\mathbf{h}_2^{\theta}||$)

Mod	Case	p_{power}
4-QAM	$0 \le \|\cos\theta_c\| \le 0.5$	q_1
	$0.5 < \|\cos\theta_c\| \le 1$	q_2
16-QAM	$0 \le \|\cos\theta_c\| \le 0.5$	q_1
	$0.5 < \|\cos\theta_c\| \le 0.866$	q_2
	$0.866 < \|\cos\theta_c\| \le 0.9$	q_5 if $\|\|\mathbf{h}_1^{\theta}\|\| \le \|\|\mathbf{h}_2^{\theta}\|\| < 3\|\|\mathbf{h}_1^{\theta}\|\|$ q_4 if $3\|\|\mathbf{h}_1^{\theta}\|\| \le \|\|\mathbf{h}_2^{\theta}\|\|$
	$0.9 < \|\cos\theta_c\| \le 0.943$	q_5 if $\|\|\mathbf{h}_1^{\theta}\|\| \le \|\|\mathbf{h}_2^{\theta}\|\| < 2\|\|\mathbf{h}_1^{\theta}\|\|$ q_4 if $2\|\|\mathbf{h}_1^{\theta}\|\| \le \|\|\mathbf{h}_2^{\theta}\|\|$
	$0.943 < \|\cos\theta_c\| \le 0.966$	q_5 if $\|\|\mathbf{h}_1^{\theta}\|\| \le \|\|\mathbf{h}_2^{\theta}\|\| < 2\|\|\mathbf{h}_1^{\theta}\|\|$ q_7 if $2\|\|\mathbf{h}_1^{\theta}\|\| \le \|\|\mathbf{h}_2^{\theta}\|\| < 3\|\|\mathbf{h}_1^{\theta}\|\|$ q_6 if $3\|\|\mathbf{h}_1^{\theta}\|\| \le \|\|\mathbf{h}_2^{\theta}\|\|$
	$0.966 < \|\cos\theta_c\| \le 0.985$	q_5 if $\|\|\mathbf{h}_1^{\theta}\|\| \le \|\|\mathbf{h}_2^{\theta}\|\| < 2\|\|\mathbf{h}_1^{\theta}\|\|$ q_6 if $2\|\|\mathbf{h}_1^{\theta}\|\| \le \|\|\mathbf{h}_2^{\theta}\|\|$
	$0.985 < \|\cos\theta_c\| \le 1$	q_6

TABLE IV
EXPRESSIONS FOR q_i IN TABLE III

q_1	$\sqrt{\frac{B}{A}}$	$A = \|\|\mathbf{h}_1^{\theta}\|\|^2 + \|\|\mathbf{h}_2^{\theta}\|\|^2$ $B = 2\|\|\mathbf{h}_2^{\theta}\|\|^2$
q_2	$\sqrt{\frac{B}{A}}$	$A = 4\|\|\mathbf{h}_1^{\theta}\|\|^2\cos^2\theta_c + \|\|\mathbf{h}_2^{\theta}\|\|^2$ $B = 2\|\|\mathbf{h}_2^{\theta}\|\|^2$
q_4	$\sqrt{\frac{-B-\sqrt{B^2-AC}}{A}}$	$A = 9\|\|\mathbf{h}_1^{\theta}\|\|^4 + \|\|\mathbf{h}_2^{\theta}\|\|^4 - 6\|\|\mathbf{h}_1^{\theta}\|\|^2\|\|\mathbf{h}_2^{\theta}\|\|^2 + 16\|\|\mathbf{h}_1^{\theta}\|\|^2\|\|\mathbf{h}_2^{\theta}\|\|^2\cos^2\theta_c$ $B = 6\|\|\mathbf{h}_1^{\theta}\|\|^2\|\|\mathbf{h}_2^{\theta}\|\|^2 - 2\|\|\mathbf{h}_2^{\theta}\|\|^4 - 16\|\|\mathbf{h}_1^{\theta}\|\|^2\|\|\mathbf{h}_2^{\theta}\|\|^2\cos^2\theta_c$ $C = 4\|\|\mathbf{h}_2^{\theta}\|\|^4$
q_5	$\sqrt{\frac{B}{A}}$	$A = 9\|\|\mathbf{h}_1^{\theta}\|\|^2 + 4\|\|\mathbf{h}_2^{\theta}\|\|^2\cos^2\theta_c$ $B = 8\|\|\mathbf{h}_2^{\theta}\|\|^2\cos^2\theta_c$
q_6	$\sqrt{\frac{-B-\sqrt{B^2-AC}}{A}}$	$A = 64\|\|\mathbf{h}_1^{\theta}\|\|^4 + \|\|\mathbf{h}_2^{\theta}\|\|^4 - 16\|\|\mathbf{h}_1^{\theta}\|\|^2\|\|\mathbf{h}_2^{\theta}\|\|^2 + 36\|\|\mathbf{h}_1^{\theta}\|\|^2\|\|\mathbf{h}_2^{\theta}\|\|^2\cos^2\theta_c$ $B = 16\|\|\mathbf{h}_1^{\theta}\|\|^2\|\|\mathbf{h}_2^{\theta}\|\|^2 - 2\|\|\mathbf{h}_2^{\theta}\|\|^4 - 36\|\|\mathbf{h}_1^{\theta}\|\|^2\|\|\mathbf{h}_2^{\theta}\|\|^2\cos^2\theta_c$ $C = 4\|\|\mathbf{h}_2^{\theta}\|\|^4$
q_7	$\sqrt{\frac{B}{A}}$	$A = 25\|\|\mathbf{h}_1^{\theta}\|\|^2 + 4\|\|\mathbf{h}_2^{\theta}\|\|^2\cos^2\theta_c$ $B = 8\|\|\mathbf{h}_2^{\theta}\|\|^2\cos^2\theta_c$

power loading for the OSM, referred to as "OSM with power loading", which was proposed in [17]. Since two matrices $\mathbf{R}_{\theta 1}$ and $\mathbf{R}_{\theta 2}$ are neglected in (8), we determine only $p = p_{power}$ by using the criteria $p_{power} = \arg\max_p d_{min}(p)$, where $d_{min}(p)$ represents the minimum distance in terms of p in the power loading system. Table III depicts the conditions for selecting the power loading parameters q_i for $||\mathbf{h}_1^{\theta}|| \le ||\mathbf{h}_2^{\theta}||$, where θ_c denotes the angle between the columns $||\mathbf{h}_1^{\theta}||$ and $||\mathbf{h}_2^{\theta}||$ of the effective channel matrix in Equation (4). For the opposite case of $||\mathbf{h}_1^{\theta}|| > ||\mathbf{h}_2^{\theta}||$, we can obtain q_i by swapping $||\mathbf{h}_1^{\theta}||$ and $||\mathbf{h}_2^{\theta}||$, and p_{power} is computed as $\sqrt{2-q_i^2}$. The values of q_i are defined in Table IV. The detailed derivations in Tables III and IV can be found in [17].

IV. SIMULATION RESULTS

In this section, we provide simulation results to demonstrate the effectiveness of the proposed precoding algorithms for OSM systems, and compare these results with the original OSM systems in [15] and [16]. The elements of the MIMO channel matrix $\overline{\mathbf{H}}$ are generated with an independent and identically distributed (i.i.d.) complex Gaussian distribution with zero mean and unit variance, whose magnitude has Rayleigh fading distribution.

In Figure 2, we compare various systems for 4-QAM constellations. In this plot, we depict the BER performance of ARITH-BER [12], *Optimal Unitary Precoding* (OUP) [13] and *Optimal Linear Precoding* (OLP) based on the minimum mean-squared error design [11]. First, we note that the performance of the proposed precoding is the same as that of the precoding presented in [18], which was shown to be optimal in terms of d_{min} in closed-loop MIMO systems. Comparing this optimum precoding with the proposed algorithm, we confirm that the proposed precoding attains the optimal performance. Note that the optimum precoding in [18] was presented in only BPSK and 4-QAM systems. Also, the receiver structure of the precoding in [18] requires joint ML detection which makes it difficult to be applied for higher modulation systems due to high computational complexity. In contrast, our precoding method is based on the symbol-by-symbol detection for arbitrary modulation levels. The required feedback amount for

Authorized licensed use limited to: IEEE Xplore. Downloaded on October 16, 2008 at 20:47 from IEEE Xplore. Restrictions apply.

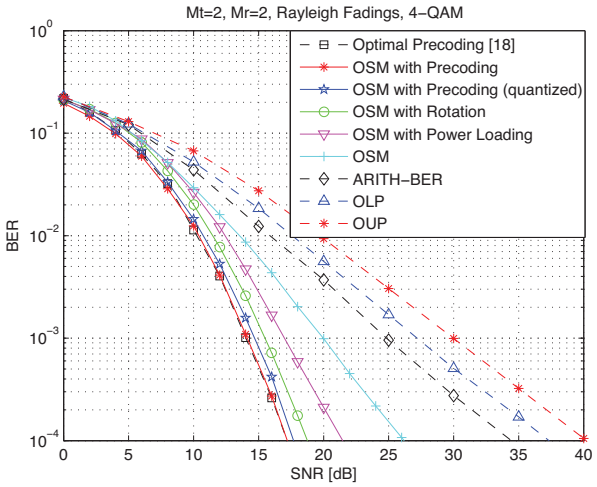

Fig. 2. BER performance of the proposed scheme with 4-QAM

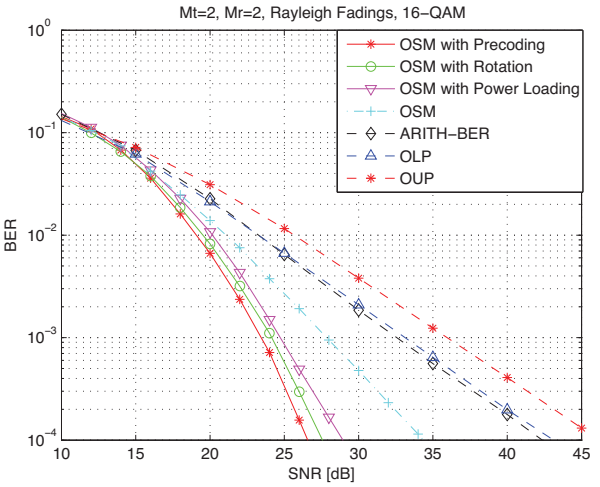

Fig. 3. BER performance of the proposed scheme with 16-QAM

the proposed precoder is also less than the system in [18]. It is interesting to note that even though the proposed scheme is based on OSM whose structure is different from the system in [18], the optimized OSM with our proposed precoder exhibits the performance identical to the optimum precoding in [18]. We can see that the proposed precoding algorithm provides a 9dB gain at a BER of 10^{-4} over the original OSM in Fig. 2. Compared to the original OSM, our precoding method additionally requires one feedback value θ_1 and one bit. Figure 2 shows that the rotation precoding and power loading precoding provide 7.5dB and 5dB gains at a BER of 10^{-4} over the original OSM, respectively. Also, we can see that ARITH-BER, OUP and OLP show a considerable performance loss compared to our proposed scheme. These performance gaps can be attributed to a fact that the proposed scheme allows a simple ML receiver, while ARITH-BER, OUP and OLP adopt linear receivers. In addition, the simulation result of the proposed scheme with quantized feedback is included. In this case, three and two bits for quantized feedback are used for θ_o and θ_1, respectively, which result in total 6 bits for feedback. Surprisingly, the quantized result show that only with 6 bits, the proposed scheme achieves the performance very close to the optimum case.

Fig. 3 shows the BER performance of various systems with 16-QAM, which are similar to those of 4-QAM in Fig. 2. We can see that the performance gain of the proposed scheme, the rotation precoding and the power loading precoding are 7.5dB, 6.5dB and 5dB at a BER of 10^{-4} over the original OSM, respectively, which are smaller compared to the 4-QAM systems. We also confirm that our proposed precoding outperforms the ARITH-BER, the OUP and the OLP.

In Fig. 4, we apply an antenna selection method to the proposed scheme with three transmit antennas and two receive antennas in 4-QAM systems. As proposed in [15] and [16], two transmit antennas can be selected out of M_t transmit antennas, based on the Euclidean distance criterion in order to maximize the system performance. In Fig. 4, the performance gains of our proposed scheme over OSM and ARITH-BER are 3dB and 4dB, respectively. The reduced performance gains compared to Fig. 2 indicate that the increased diversity gain from more transmitter antennas is more beneficial to OSM, ARITH-BER, OLP and OUP. Also, the quantized feedback

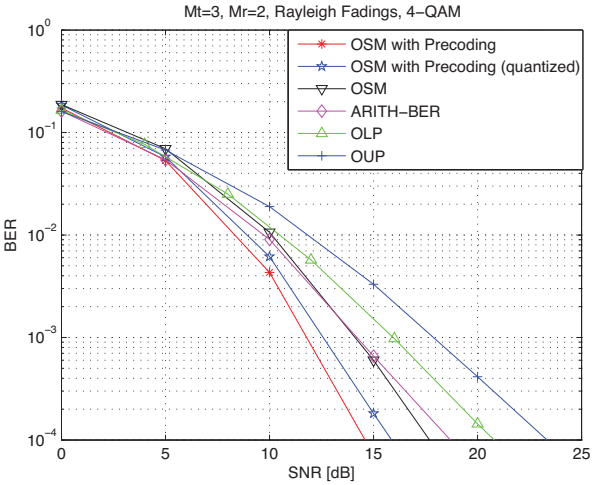

Fig. 4. BER performance of the proposed scheme with 4-QAM in 3×2 systems

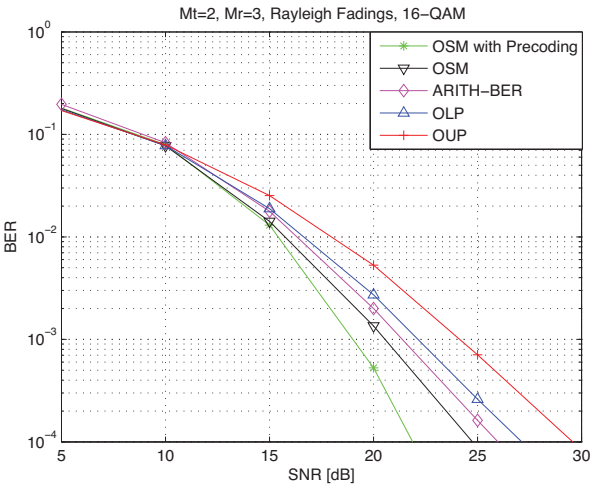

Fig. 5. BER performance of the proposed scheme with 16-QAM in 2×3 systems

Authorized licensed use limited to: IEEE Xplore. Downloaded on October 16, 2008 at 20:47 from IEEE Xplore. Restrictions apply.

result with the same quantization bits as in Fig. 2 is plotted, which is only 1dB away from the unquantized case. It is expected to require more quantized bits for feedback in higher modulation levels.

Finally, we depict the proposed scheme with two transmit and three receive antennas in a 16-QAM system in Fig. 5. The BER improvements of the proposed scheme are 3dB, 4dB, 5dB and 7.5dB in comparison to the original OSM, ARITH-BER, OLP and OUP, respectively. The performance gain, due to the increased receive antenna diversity, becomes more pronounced in the conventional systems.

V. Conclusion

In this paper, we have presented a new precoding algorithm for the OSM scheme in MIMO systems, which gives an excellent performance improvement with additional feedback information. Our algorithm maximizes the minimum Euclidean distance to enhance the system performance. We have illustrated a partitioning approach to determine the optimal precoding parameters which maximize the minimum Euclidean distance between the constellation points in the effective channel in OSM systems. The derivation shows that our proposed precoder requires one real value and two bits for feedback for 16-QAM. The simulation results confirm that the proposed algorithm for the OSM is optimal in terms of the minimum distance in closed-loop MIMO systems. We can extend the proposed algorithm to higher level modulations. Also, the proposed scheme can be applied to systems which support more than two data streams by employing a method presented in [21].

Appendix A
Analysis for 4-QAM

For 4-QAM constellations, we consider that the real or imaginary part of the transmitted symbol is equal to $\pm\frac{1}{2}$. From the system model (6), the noiseless received symbols in the effective channel become $(\mathbf{h}^{\theta}_{1p}+\mathbf{h}^{\theta}_{2p})/2$, $(-\mathbf{h}^{\theta}_{1p}+\mathbf{h}^{\theta}_{2p})/2$, $(-\mathbf{h}^{\theta}_{1p}-\mathbf{h}^{\theta}_{2p})/2$ and $(\mathbf{h}^{\theta}_{1p}-\mathbf{h}^{\theta}_{2p})/2$. Then, the optimization criterion (12) is equivalent to

$$(p_{opt},\ \theta_{2opt}) = \arg \max_{0\le p\le\sqrt{2},\ 0\le\theta_2\le\pi/4} \{\min(||\mathbf{h}^{\theta}_{1p}||,\ ||\mathbf{h}^{\theta}_{2p}||, ||\mathbf{h}^{\theta}_{1p}+\mathbf{h}^{\theta}_{2p}||,\ ||\mathbf{h}^{\theta}_{1p}-\mathbf{h}^{\theta}_{2p}||)\}.$$

where we have

$$\begin{aligned}
||\mathbf{h}^{\theta}_{1p}||^2 &= ||\mathbf{h}^{\theta}_{1R}||^2 p^2\cos^2\theta_2 + ||\mathbf{h}^{\theta_2}_{2R}||^2(2-p)^2\sin^2\theta_2\\
||\mathbf{h}^{\theta}_{2p}||^2 &= ||\mathbf{h}^{\theta}_{1R}||^2 p^2\sin^2\theta_2 + ||\mathbf{h}^{\theta}_{2R}||^2(2-p)^2\cos^2\theta_2\\
||\mathbf{h}^{\theta}_{1p}+\mathbf{h}^{\theta}_{2p}||^2 &= ||\mathbf{h}^{\theta}_{1R}||^2 p^2(\cos^2\theta_2+\sin^2\theta_2-2\sin\theta_2\cos\theta_2)\\
&\quad +||\mathbf{h}^{\theta}_{2R}||^2(2-p)^2(\sin^2\theta_2+\cos^2\theta_2+2\sin\theta_2\cos\theta_2)\\
||\mathbf{h}^{\theta}_{1p}-\mathbf{h}^{\theta}_{2p}||^2 &= ||\mathbf{h}^{\theta}_{1R}||^2 p^2(\cos^2\theta_2+\sin^2\theta_2+2\sin\theta_2\cos\theta_2)\\
&\quad +||\mathbf{h}^{\theta}_{2R}||^2(2-p)^2(\sin^2\theta_2+\cos^2\theta_2-2\sin\theta_2\cos\theta_2).
\end{aligned} \quad \text{(A-1)}$$

Now we adopt a "divide-and-conquer" approach to facilitate the optimization process in (12). Instead of identifying p and θ_2 which maximize (12) for the whole region, the search area of $0\le p\le\sqrt{2}$ and $0\le\theta_2\le\pi/4$ is divided into three partitions as shown in Fig. 6. These partitions are made such that the number of candidates of d_{min} is minimized. Note that the candidate functions of d_{min} within each partition are either a monotonically increasing or decreasing function with respect to θ_2, for a fixed value p. Now, we will find p and θ_2 which maximize d_{min} in each partition. Since θ_1 is already computed so as to maximize $||\mathbf{h}^{\theta}_{1R}||$, we have $||\mathbf{h}^{\theta}_{1R}||^2 \ge ||\mathbf{h}^{\theta}_{2R}||^2$. Thus, defining k as $||\mathbf{h}^{\theta}_{1R}||^2/||\mathbf{h}^{\theta}_{2R}||^2$, this leads to $k\ge 1$. Then, after finding the maximum value of d_{min} in each partition, we can identify p and θ_2 which maximize d_{min} for the whole region. Let us start with the partition A_4^2.

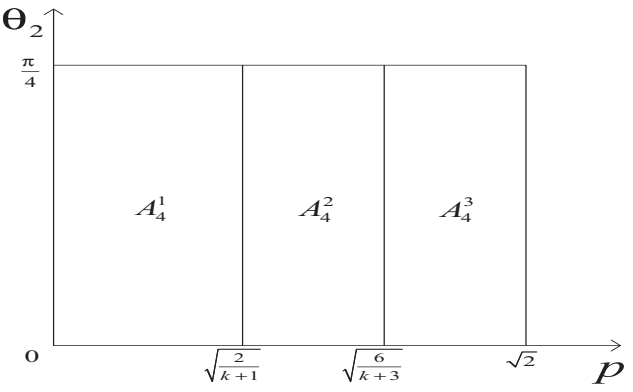

Fig. 6. Partition areas for the optimal precoding in the proposed system with 4-QAM

1) Partition A_4^2 $\left(\sqrt{2/(k+1)}\le p\le\sqrt{6/(k+3)}, 0\le\theta_2\le\pi/4\right)$

With this partition, it is easy to see that $||\mathbf{h}^{\theta}_{1R}||^2p^2 \ge ||\mathbf{h}^{\theta}_{2R}||^2(2-p^2)$. Using this and Equation (A-1), we have the following relations: $||\mathbf{h}^{\theta}_{1p}||^2 \ge ||\mathbf{h}^{\theta}_{2p}||^2$, $||\mathbf{h}^{\theta}_{1p}-\mathbf{h}^{\theta}_{2p}||^2 \ge ||\mathbf{h}^{\theta}_{1p}+\mathbf{h}^{\theta}_{2p}||^2$ and $||\mathbf{h}^{\theta}_{1p}+\mathbf{h}^{\theta}_{2p}||^2 \ge ||\mathbf{h}^{\theta}_{2p}||^2$. This means that d_{min} is equal to $||\mathbf{h}^{\theta}_{2p}||$ in this partition, regardless of p and θ_2. For a given θ_2, $||\mathbf{h}^{\theta}_{2p}||^2$ is a monotonically increasing function of p for $\sqrt{2/(k+1)}\le p\le\sqrt{6/(k+3)}$. Also, for a given p, $||\mathbf{h}^{\theta}_{2p}||^2$ is a monotonically increasing function of θ_2 for $0\le\theta_2\le\pi/4$. As a result, to maximize d_{min}, p and θ_2 must be $\sqrt{6/(k+3)}$ and $\pi/4$, respectively, and for these values, we have $d^2_{min}=4k||\mathbf{h}^{\theta}_{2R}||^2/(k+3)$.

2) Partition A_4^3 $\left(\sqrt{6(k+3)}\le p\le\sqrt{2},\quad 0\le\theta_2\le\pi/4\right)$

In this partition, we have $||\mathbf{h}^{\theta}_{1p}||^2 \ge ||\mathbf{h}^{\theta}_{2p}||^2$ and $||\mathbf{h}^{\theta}_{1p}-\mathbf{h}^{\theta}_{2p}||^2 \ge ||\mathbf{h}^{\theta}_{1p}+\mathbf{h}^{\theta}_{2p}||^2$. Then, the candidates for d_{min} are $||\mathbf{h}^{\theta}_{2p}||$ and $||\mathbf{h}^{\theta}_{1p}+\mathbf{h}^{\theta}_{2p}||$. Following the analysis method described in Appendix C, we can show that the case of $||\mathbf{h}^{\theta}_{2p}||^2=||\mathbf{h}^{\theta}_{1p}+\mathbf{h}^{\theta}_{2p}||^2$ maximizes d_{min} in this partition. By solving this equality, θ_2 can be expressed as (See Appendix D for proof.)

$$\theta_2=\sin^{-1}\sqrt{\frac{3kp^2-2(2-p^2)-\sqrt{(3kp^2-2(2-p^2))^2-5k^2p^4}}{5(kp^2-(2-p^2))}}. \quad \text{(A-2)}$$

The other solution of θ_2 shown in Appendix D is not considered, since it does not belong to this partition ($0\le\theta_2\le\pi/4$).

Substituting Eq. (A-2) into Eq. (A-1) yields

$$||\mathbf{h}^{\theta}_{2p}||^2 = \frac{3(k-1)p^2+6-\sqrt{(3kp^2-2(2-p^2))^2-5k^2p^4}}{5}||\mathbf{h}^{\theta}_{2R}||^2. \quad \text{(A-3)}$$

To identify the maximum value of Equation (A-3), we need to find the derivative of (A-3) with respect to p, which is given

Authorized licensed use limited to: IEEE Xplore. Downloaded on October 16, 2008 at 20:47 from IEEE Xplore. Restrictions apply.

by

$$\frac{d}{dp}||\mathbf{h}_{2p}^{\theta}||^2 = \frac{2p}{5}\left(3(k-1) - \frac{(4k^2+12k+4)p^2-(12k+8)}{\sqrt{(4k^2+12k+4)p^4-2(12k+8)p^2+16}}\right) = 0. \quad \text{(A-4)}$$

Then, rearranging Equation (A-4) results in

$$(k^2-6k+1)(k^2+3k+1)p^4 - 2(3k+2)(k^2-6k+1)p^2 + 4(-6k+1) = 0. \quad \text{(A-5)}$$

Equation (A-5) is a quadratic equation of p^2 and the roots of the equation can be obtained as

$$p^2 = \frac{(3k+2)(k^2-6k+1) \pm \sqrt{9k^2(k^2-6k+1)(k-1)^2}}{(k^2-6k+1)(k^2+3k+1)}. \quad \text{(A-6)}$$

Using Equations (A-5) and (A-6), we recognize that p must be on the boundary of this partition to maximize d_{min}, which is equal to $||\mathbf{h}_{2p}^{\theta}||^2$. Thus, p should be either $\sqrt{6/(k+3)}$ or $\sqrt{2}$ to maximize Equation (A-3). Correspondingly, θ_2 is either $\pi/4$ or 0.464 and d_{min}^2 is $4k||\mathbf{h}_{2R}^{\theta}||^2/(k+3)$ or $2k||\mathbf{h}_{2R}^{\theta}||^2/5$. It is interesting to note that θ_2 is independent of k.

3) Partition A_4^1 $\left(0 \le p \le \sqrt{2/(k+1)},\ \ 0 \le \theta_2 \le \pi/4\right)$

In this partition, since $\mathbf{h}_{1R}^{\theta}$ is made smaller than $\mathbf{h}_{2R}^{\theta}$ for the range of p, we have a smaller maximum value of d_{min} than the other partitions. Thus, we do not consider this partition.

APPENDIX B
ANALYSIS FOR 16-QAM

For 16-QAM constellations, we consider that the real or imaginary part of the transmitted symbol equals $\pm\frac{1}{2}$ or $\pm\frac{3}{2}$. Then, the candidates of d_{min} are given as follows: $||\mathbf{h}_{1p}^{\theta}||$, $||\mathbf{h}_{2p}^{\theta}||$, $||\mathbf{h}_{1p}^{\theta}-\mathbf{h}_{2p}^{\theta}||$, $||\mathbf{h}_{1p}^{\theta}+\mathbf{h}_{2p}^{\theta}||$, $||\mathbf{h}_{1p}^{\theta}-2\mathbf{h}_{2p}^{\theta}||$, $||\mathbf{h}_{1p}^{\theta}+2\mathbf{h}_{2p}^{\theta}||$, $||2\mathbf{h}_{1p}^{\theta}-\mathbf{h}_{2p}^{\theta}||$, $||2\mathbf{h}_{1p}^{\theta}+\mathbf{h}_{2p}^{\theta}||$, $||\mathbf{h}_{1p}^{\theta}-3\mathbf{h}_{2p}^{\theta}||$, $||\mathbf{h}_{1p}^{\theta}+3\mathbf{h}_{2p}^{\theta}||$, $||3\mathbf{h}_{1p}^{\theta}-\mathbf{h}_{2p}^{\theta}||$, $||3\mathbf{h}_{1p}^{\theta}+\mathbf{h}_{2p}^{\theta}||$, $||3\mathbf{h}_{1p}^{\theta}-2\mathbf{h}_{2p}^{\theta}||$, $||3\mathbf{h}_{1p}^{\theta}+2\mathbf{h}_{2p}^{\theta}||$, $||2\mathbf{h}_{1p}^{\theta}-3\mathbf{h}_{2p}^{\theta}||$, $||2\mathbf{h}_{1p}^{\theta}+3\mathbf{h}_{2p}^{\theta}||$. The area enclosed by $0 \le p \le \sqrt{2}$ and $0 \le \theta_2 \le \pi/4$ is divided into nine partitions as shown in Fig. 7. Similar to the 4-QAM case in Appendix A, the boundary points of θ_2 in Fig. 7 are chosen such that all of the candidates of d_{min} within each partition are either monotonically increasing or decreasing functions with respect to θ_2, for a fixed value p. Then, given the boundary points of θ_2, we determine the boundary points of p to reduce the number of candidates of d_{min}.

First, because of a similar reason as in the A_4^1 case of Appendix A, A_{16}^1 is not considered. Then, using the inequality $||\mathbf{h}_{1R}^{\theta}||^2p^2 \ge ||\mathbf{h}_{2R}^{\theta}||^2(2-p^2)$, which is common to partitions A_{16}^i $(i = 2, ..., 9)$, the candidates of d_{min} reduce to $||\mathbf{h}_{1p}^{\theta}||$, $||\mathbf{h}_{1p}^{\theta}+\mathbf{h}_{2p}^{\theta}||$, $||\mathbf{h}_{1p}^{\theta}+2\mathbf{h}_{2p}^{\theta}||$ and $||\mathbf{h}_{1p}^{\theta}+3\mathbf{h}_{2p}^{\theta}||$. Here, to simplify the analysis we will not consider $||2\mathbf{h}_{1p}^{\theta}+3\mathbf{h}_{2p}^{\theta}||$, since simulation results show that $||2\mathbf{h}_{1p}^{\theta}+3\mathbf{h}_{2p}^{\theta}||$ is not a dominant factor. Then, we have

$$\begin{aligned}
||\mathbf{h}_{2p}^{\theta}||^2 &= ||\mathbf{h}_{1R}^{\theta}||^2p^2\sin^2\theta_2 + ||\mathbf{h}_{2R}^{\theta}||^2(2-p)^2\cos^2\theta_2 \\
||\mathbf{h}_{1p}^{\theta}+\mathbf{h}_{2p}^{\theta}||^2 &= ||\mathbf{h}_{1R}^{\theta}||^2p^2(\cos^2\theta_2+\sin^2\theta_2-2\sin\theta_2\cos\theta_2) \\
&\quad + ||\mathbf{h}_{2R}^{\theta}||^2(2-p)^2(\sin^2\theta_2+\cos^2\theta_2+2\sin\theta_2\cos\theta_2) \\
||\mathbf{h}_{1p}^{\theta}+2\mathbf{h}_{2p}^{\theta}||^2 &= ||\mathbf{h}_{1R}^{\theta}||^2p^2(\cos^2\theta_2+4\sin^2\theta_2-4\sin\theta_2\cos\theta_2) \\
&\quad + ||\mathbf{h}_{2R}^{\theta}||^2(2-p)^2(\sin^2\theta_2+4\cos^2\theta_2+4\sin\theta_2\cos\theta_2) \\
||\mathbf{h}_{1p}^{\theta}+3\mathbf{h}_{2p}^{\theta}||^2 &= ||\mathbf{h}_{1R}^{\theta}||^2p^2(\cos^2\theta_2+9\sin^2\theta_2-6\sin\theta_2\cos\theta_2) \\
&\quad + ||\mathbf{h}_{2R}^{\theta}||^2(2-p)^2(\sin^2\theta_2+9\cos^2\theta_2+6\sin\theta_2\cos\theta_2).
\end{aligned} \quad \text{(A-7)}$$

Now, we start with the partitions A_{16}^8, A_{16}^5 and A_{16}^2.

1) Partitions A_{16}^8 $\left(\sqrt{2/(k+1)} \le p \le \sqrt{182/(k+91)},\ 0 \le \theta_2 \le 0.322\right)$, A_{16}^5 $\left(\sqrt{2/(k+1)} \le p \le \sqrt{42/(k+21)},\ 0.322 \le \theta_2 \le 0.464\right)$ and A_{16}^2 $\left(\sqrt{\frac{2}{k+1}} \le p \le \sqrt{\frac{6}{k+3}},\ 0.464 \le \theta_2 \le \pi/4\right)$

Using a method in Appendix C, we can check that d_{min}^2 equals $||\mathbf{h}_{2p}^{\theta}||^2$ in the partition A_{16}^8, regardless of p and θ_2. Since $||\mathbf{h}_{2p}^{\theta}||^2$ is a monotonically increasing function of θ_2 for a fixed value of p, $\theta_2 = 0.322$ maximizes d_{min}. Then, for this given θ_2, $||\mathbf{h}_{2p}^{\theta}||^2$ is a monotonically decreasing function of p for $1 \le k \le 9$, while $||\mathbf{h}_{2p}^{\theta}||^2$ is a monotonically increasing function of p for $k > 9$. Thus, in the partition A_{16}^8, p and θ_2 which maximize d_{min}^2, can be obtained as

$$\begin{cases} p = \sqrt{2/(k+1)}, & \theta_2 = 0.322 \\ d_{min}^2 = 2k||\mathbf{h}_{2R}^{\theta}||^2/(k+1) & \text{if } \ 1 \le k \le 9 \\ p = \sqrt{182/(k+91)}, & \theta_2 = 0.322 \\ d_{min}^2 = 20k||\mathbf{h}_{2R}^{\theta}||^2/(k+91) & \text{if } \ k > 9\ . \end{cases}$$

Also, by applying this solution to the partitions A_{16}^5 and A_{16}^2, we obtain the solution for p and θ_2 for each partition. For A_{16}^5, we have

$$\begin{cases} p = \sqrt{2/(k+1)}, & \theta_2 = 0.464 \\ d_{min}^2 = 2k||\mathbf{h}_{2R}^{\theta}||^2/(k+1) & \text{if } \ 1 \le k \le 4 \\ p = \sqrt{42/(k+21)}, & \theta_2 = 0.464 \\ d_{min}^2 = 10k||\mathbf{h}_{2R}^{\theta}||^2/(k+21) & \text{if } \ k > 4\ . \end{cases}$$

and for A_{16}^2, we obtain

$$p = \sqrt{6/(k+3)}\ \ \theta_2 = \pi/4, \ \text{and } d_{min}^2 = 4k||\mathbf{h}_{2R}^{\theta}||^2/(k+3).$$

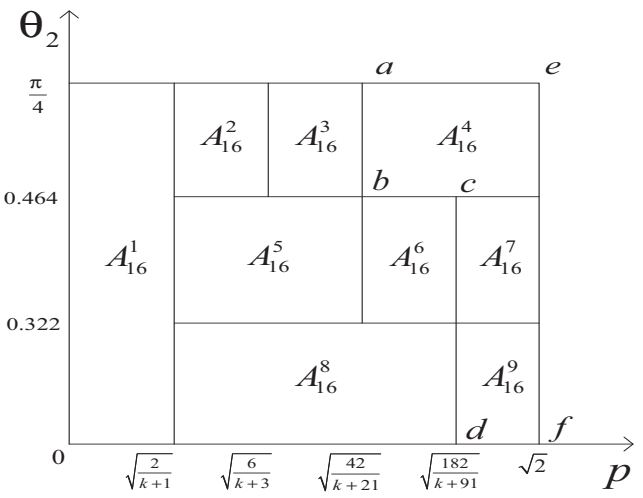

Fig. 7. Partitions for the proposed optimal precoding with 16-QAM

Authorized licensed use limited to: IEEE Xplore. Downloaded on October 16, 2008 at 20:47 from IEEE Xplore. Restrictions apply.

2) Partitions A_{16}^6 $\left(\sqrt{42/(k+21)} \le p \le \sqrt{182/(k+91)},\ 0.322 \le \theta_2 \le 0.464\right)$ and A_{16}^3 $\left(\sqrt{6/(k+3)} \le p \le \sqrt{42/(k+21)},\ \ 0.464 \le \theta_2 \le \pi/4\right)$

Based on the analysis in Appendix C, it can be shown that the candidates of d_{min} are $||\mathbf{h}_{2p}^{\theta}||^2$ and $||\mathbf{h}_{1p}^{\theta}+\mathbf{h}_{2p}^{\theta}||^2$. Also, $||\mathbf{h}_{2p}^{\theta}||^2$ should be equal to $||\mathbf{h}_{1p}^{\theta}+\mathbf{h}_{2p}^{\theta}||^2$ in the partition A_{16}^6 to maximize d_{min}. Solving $||\mathbf{h}_{2p}^{\theta}||^2 = ||\mathbf{h}_{1p}^{\theta}+\mathbf{h}_{2p}^{\theta}||^2$ from the result in Appendix D, θ_2 is expressed as

$$\theta_2 = \sin^{-1}\left(\left(\frac{3kp^2-7(2-p^2)}{10(kp^2-(2-p^2))} - \frac{\sqrt{(3kp^2-7(2-p^2))^2-5(kp^2+3(2-p^2))^2}}{10(kp^2-(2-p^2))}\right)^{\frac{1}{2}}\right). \quad \text{(A-8)}$$

Using a similar analysis in the partition A_4^3 of Appendix A, we notice that p should be on the boundary of this partition $\left(p = \sqrt{42/(k+21)}\right.$ or $\left.\sqrt{182/(k+91)}\right)$. Then, substituting each value of p into Equation (A-8) yields $\theta_2 = 0.464$ and 0.345, and these values correspond to $d_{min}^2 = 10k||\mathbf{h}_{2R}^{\theta}||^2/(k+21)$ and $22.592k||\mathbf{h}_{2R}^{\theta}||^2/(k+91)$, respectively.

Also, in the partition A_{16}^3, following a similar step as in the partition A_4^3 of Appendix A, p should be on the boundary of this partition ($p = \sqrt{6/(k+3)}$ or $\sqrt{42/(k+21)}$). These two values of p result in $\theta_2 = \pi/4$ or 0.489, and we have $d_{min}^2 = 4k||\mathbf{h}_{2R}^{\theta}||^2/(k+3)$ or $10.8k||\mathbf{h}_{2R}^{\theta}||^2/(k+21)$, respectively.

3) Partitions A_{16}^9 $\left(\sqrt{182/(k+91)} \le p \le \sqrt{2},\ 0 \le \theta_2 \le 0.322\right)$, A_{16}^7 $\left(\sqrt{182/(k+91)} \le p \le \sqrt{2},\ 0.322 \le \theta_2 \le 0.464\right)$ and A_{16}^4 $\left(\sqrt{42/(k+21)} \le p \le \sqrt{2},\ \ 0.464 \le \theta_2 \le \pi/4\right)$

In these partitions, the candidates for d_{min} consist of more than two functions. Utilizing results from Appendix C, we can find that the candidates for A_{16}^9,A_{16}^7 and A_{16}^4 are $\{||\mathbf{h}_{2p}^{\theta}||^2, ||\mathbf{h}_{1p}^{\theta}+3\mathbf{h}_{2p}^{\theta}||^2\}$, $\{||\mathbf{h}_{2p}^{\theta}||^2, ||\mathbf{h}_{1p}^{\theta}+2\mathbf{h}_{2p}^{\theta}||^2, ||\mathbf{h}_{1p}^{\theta}+3\mathbf{h}_{2p}^{\theta}||^2\}$ and $\{||\mathbf{h}_{2p}^{\theta}||^2, ||\mathbf{h}_{1p}^{\theta}+\mathbf{h}_{2p}^{\theta}||^2, ||\mathbf{h}_{1p}^{\theta}+2\mathbf{h}_{2p}^{\theta}||^2\}$, respectively. Also, based on the results in Appendix C, we need to satisfy the relations $||\mathbf{h}_{2p}^{\theta}||^2 = ||\mathbf{h}_{1p}^{\theta}+3\mathbf{h}_{2p}^{\theta}||^2$ in A_{16}^9, $||\mathbf{h}_{2p}^{\theta}||^2 = ||\mathbf{h}_{1p}^{\theta}+2\mathbf{h}_{2p}^{\theta}||^2$ or $||\mathbf{h}_{1p}^{\theta}+2\mathbf{h}_{2p}^{\theta}||^2 = ||\mathbf{h}_{1p}^{\theta}+3\mathbf{h}_{2p}^{\theta}||^2$ in A_{16}^7 and $||\mathbf{h}_{2p}^{\theta}||^2 = ||\mathbf{h}_{1p}^{\theta}+\mathbf{h}_{2p}^{\theta}||^2$ or $||\mathbf{h}_{1p}^{\theta}+\mathbf{h}_{2p}^{\theta}||^2 = ||\mathbf{h}_{1p}^{\theta}+2\mathbf{h}_{2p}^{\theta}||^2$ in A_{16}^4. By using a similar process in A_4^3 of Appendix A, we notice that p should be on the boundary $\overline{ab}$, $\overline{cd}$ or $\overline{ef}$ in Fig. 7 when all of the above equalities hold. Since we have already analyzed the condition on $\overline{ab}$ and $\overline{cd}$ at the partitions A_{16}^8, A_{16}^6 and A_{16}^3, we only need to evaluate the boundary $\overline{ef}$ ($p = \sqrt{2}$). Unlike other partitions, we do not know which equality maximizes d_{min}, except for the fact that p equals $\sqrt{2}$. Substituting $p = \sqrt{2}$ into Equation (A-7) yields

$$\begin{aligned}
&||\mathbf{h}_{2p}^{\theta}||^2 = 2||\mathbf{h}_{1R}^{\theta}||^2 \sin^2\theta_2 \\
&||\mathbf{h}_{1p}^{\theta}+\mathbf{h}_{2p}^{\theta}||^2 = 2||\mathbf{h}_{1R}^{\theta}||^2(\cos^2\theta_2+\sin^2\theta_2-2\sin\theta_2\cos\theta_2) \quad \text{(A-9)} \\
&||\mathbf{h}_{1p}^{\theta}+2\mathbf{h}_{2p}^{\theta}||^2 = 2||\mathbf{h}_{1R}^{2\theta}||^2(\cos^2\theta_2+4\sin^2\theta_2-4\sin\theta_2\cos\theta_2) \\
&||\mathbf{h}_{1p}^{\theta}+3\mathbf{h}_{2p}^{\theta}||^2 = 2||\mathbf{h}_{1R}^{\theta}||^2(\cos^2\theta_2+9\sin^2\theta_2-6\sin\theta_2\cos\theta_2).
\end{aligned}$$

After some mathematical manipulations, it can be shown that $||\mathbf{h}_{2p}^{\theta}||^2$ should be equal to $||\mathbf{h}_{1p}^{\theta}+3\mathbf{h}_{2p}^{\theta}||^2$ to maximize d_{min}. Then, θ_2 can be obtained from Appendix D as a solution of $||\mathbf{h}_{2p}^{\theta}||^2 = ||\mathbf{h}_{1p}^{\theta}+3\mathbf{h}_{2p}^{\theta}||$ as

$$\theta_2 = \sin^{-1}\left(\left(\frac{11kp^2-74(2-p^2)}{85(kp^2-(2-p^2))} - \frac{\sqrt{(11kp^2-74(2-p^2))^2-85(kp^2+8(2-p^2))^2}}{10(kp^2-(2-p^2))}\right)^{\frac{1}{2}}\right). \quad \text{(A-10)}$$

Again, by plugging $p = \sqrt{2}$ into Equation (A-10), we obtain $\theta_2 = 0.245$. Also, we have $d_{min}^2 = 2k||\mathbf{h}_{2R}^{\theta}||^2/17$.

APPENDIX C

In this appendix, we present a systemic way of reducing the number of candidates of d_{min} for a given partition. First, for each partition, by taking the derivatives of the candidate functions with respect to θ_2 with a fixed value p, we determine whether it is an increasing or a decreasing function. Note that each partition is determined such that the candidate functions within the partition are either monotonically increasing or monotonically decreasing functions with respect to θ_2 for a fixed value p. Next, we evaluate the inequality among the candidates at two end values of θ_2 for the given partition. Then, the number of candidates of d_{min} is reduced by comparing each candidate function with respect to θ_2.

To illustrate the above method, we present the process of determining the candidates in the partition A_{16}^4 as an example. First, as mentioned in Section II, the candidates of d_{min} in 16-QAM are $||\mathbf{h}_{1p}^{\theta}||$, $||\mathbf{h}_{1p}^{\theta}+\mathbf{h}_{2p}^{\theta}||$, $||\mathbf{h}_{1p}^{\theta}+2\mathbf{h}_{2p}^{\theta}||$ and $||\mathbf{h}_{1p}^{\theta}+3\mathbf{h}_{2p}^{\theta}||$. After differentiating the candidate functions with respect to θ_2, we determine that $||\mathbf{h}_{2p}^{\theta}||^2$, $||\mathbf{h}_{1p}^{\theta}+2\mathbf{h}_{2p}^{\theta}||^2$ and $||\mathbf{h}_{1p}^{\theta}+3\mathbf{h}_{2p}^{\theta}||^2$ are monotonically increasing functions, while $||\mathbf{h}_{1p}^{\theta}+\mathbf{h}_{2p}^{\theta}||^2$ is a monotonically decreasing function. Next, by substituting two end values of θ_2 (0.464 and $\pi/4$) into the candidate functions in A_{16}^4, the following inequalities are obtained:

$$\begin{aligned}
&\theta_2 = \pi/4 \ : \\
&||\mathbf{h}_{1p}^{\theta}+3\mathbf{h}_{2p}^{\theta}||^2 \ge ||\mathbf{h}_{1p}^{\theta}+2\mathbf{h}_{2p}^{\theta}||^2 \ge ||\mathbf{h}_{2p}^{\theta}||^2 \ge ||\mathbf{h}_{1p}^{\theta}+\mathbf{h}_{2p}^{\theta}||^2 \\
&\theta_2 = 0.464 \ : \\
&||\mathbf{h}_{1p}^{\theta}+3\mathbf{h}_{2p}^{\theta}||^2 \ge ||\mathbf{h}_{1p}^{\theta}+\mathbf{h}_{2p}^{\theta}||^2 \ge ||\mathbf{h}_{2p}^{\theta}||^2 \ge ||\mathbf{h}_{1p}^{\theta}+2\mathbf{h}_{2p}^{\theta}||^2.
\end{aligned}$$

Then, plotting the candidate functions based on the above relations, we notice that only two cases are possible as depicted in Figs. 8 (a) and (b). From this plot, we confirm that $||\mathbf{h}_{1p}^{\theta}+3\mathbf{h}_{2p}^{\theta}||$ cannot be the minimum distance. For the case of Fig. 8 (a), the maximum of d_{min} is obtained at $\theta_2 = \theta_2'$ where $||\mathbf{h}_{1p}^{\theta}+\mathbf{h}_{2p}^{\theta}||^2 = ||\mathbf{h}_{1p}^{\theta}+2\mathbf{h}_{2p}^{\theta}||^2$. Also, we can recognize that for the case of Fig. 8 (b), d_{min} is maximized when we have $||\mathbf{h}_{2p}^{\theta}||^2 = ||\mathbf{h}_{1p}^{\theta}+\mathbf{h}_{2p}^{\theta}||^2$ at $\theta_2 = \theta_2''$. This analysis leads to a conclusion that to maximize d_{min}, θ_2 should be determined such that we have $||\mathbf{h}_{1p}^{\theta}+\mathbf{h}_{2p}^{\theta}||^2 = ||\mathbf{h}_{1p}^{\theta}+2\mathbf{h}_{2p}^{\theta}||^2$ or $||\mathbf{h}_{2p}^{\theta}||^2 = ||\mathbf{h}_{1p}^{\theta}+\mathbf{h}_{2p}^{\theta}||^2$.

APPENDIX D

As can be seen from the analysis in Appendix A, most partitions need to solve an equation in the form of $||a\mathbf{h}_{1p}^{\theta}+b\mathbf{h}_{2p}^{\theta}|| = ||c\mathbf{h}_{1p}^{\theta}+d\mathbf{h}_{2p}^{\theta}||$, where a, b, c and d denote integer

Authorized licensed use limited to: IEEE Xplore. Downloaded on October 16, 2008 at 20:47 from IEEE Xplore. Restrictions apply.

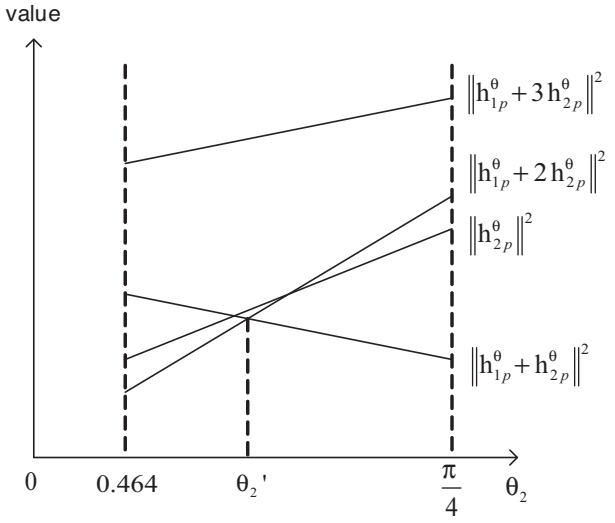

(a)

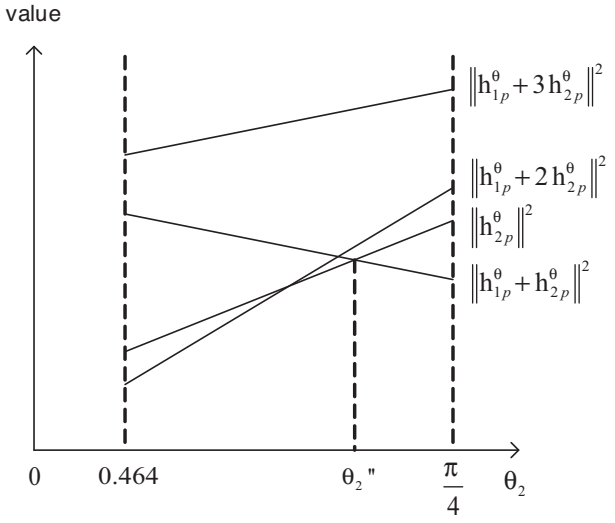

(b)

Fig. 8. d_{min}^2 of candidates with fixed p in A_{16}^4

numbers. To solve the equation $||a\mathbf{h}_{1p}^{\theta}+b\mathbf{h}_{2p}^{\theta}||^2=||c\mathbf{h}_{1p}^{\theta}+d\mathbf{h}_{2p}^{\theta}||^2$, it follows

$$||\mathbf{h}_{1R}^{\theta}||^2p^2((a^2-c^2)\cos^2\theta_2-2(ab-cd)\sin\theta_2\cos\theta_2+(b^2-d^2)\sin^2\theta_2)+||\mathbf{h}_{2R}^{\theta}||^2(2-p^2)((a^2-c^2)\sin^2\theta_2+2(ab-cd)\sin\theta_2\cos\theta_2+(b^2-d^2)\cos^2\theta_2)=0.$$

The solution of the above equation is given by

$$\theta_2=\sin^{-1}\sqrt{\frac{B\pm\sqrt{B^2-AC}}{A}}$$

where $A=(kp^2-(2-p^2))^2((b^2-d^2-a^2+c^2)^2+4(ab-cd)^2)$, $B=(kp^2-(2-p^2))((kp^2(a^2-c^2)+(2-p^2)(b^2-d^2))(-b^2+d^2+a^2-c^2)+2(ab-cd)^2(kp^2-(2-p^2)))$ and $C=(kp^2(a^2-c^2)+(2-p^2)(b^2-d^2))^2$.

REFERENCES

[1] A. J. Paulraj, D. A. Gore, R. U. Nabar, and H. Bölcskei, "An overview of MIMO communications-A key to gigabit wireless," in *Proc. IEEE*, vol. 92, pp. 198–218, February 2004.

[2] G. J. Foschini and M. Gans, "On Limits of Wireless Communications in a Fading Environment when Using Multiple Antennas," *Wireless Personal Communications*, vol. 6, pp. 311–335, March 1998.

[3] I. E. Telatar, "Capacity of multi-antenna Gaussian channels," *Eur. Trans. Telecom.*, vol. 10, pp. 585–595, November 1999.

[4] S. M. Alamouti, "A simple transmit diversity techniques for wireless communications," *IEEE Journal on Selected Areas in Communications*, vol. 16, pp. 1451–1458, October 1998.

[5] V. Tarokh, N. Seshadri, and A. R. Calderbank, "Space-time codes for high data rate wireless communication: performance criterion and code construction," *IEEE Transactions on Information Theory*, vol. IT-44, pp. 744–765, March 1998.

[6] V. Tarokh, H. Jafarkhani, and A. R. Calderbank, "Space-time block codes from orthogonal designs," *IEEE Transactions on Information Theory*, vol. 45, pp. 1456–1467, July 1999.

[7] G. J. Foschini, "Layered space-time architecture for wireless communication in a fading environment when using multi-element antennas," *Bell Labs. Tech. J.*, vol. 1, pp. 41–59, 1996.

[8] G. J. Foschini, G. D. Golden, R. A. Valenzuela, and P. W. Wolniansky, "Simplified Processing for High Spectral Efficiency Wireless Communication Employing Multi-Element Arrays," *IEEE Journal on Selected Areas in Communications*, vol. 17, pp. 1841–1852, November 1999.

[9] G. J. Foschini, D. Chizhik, M. J. Gans, C. Papadias, and R. A. Valenzuela, "Analysis and Performance of Some Basic Space-Time Architectures," *IEEE Journal on Selected Areas in Communications*, vol. 21, pp. 303–320, April 2003.

[10] G. G. Raleigh and J. M. Cioffi, "Spatio-Temporal Coding for Wireless Communication," *IEEE Transactions on Communications*, vol. 46, pp. 357–366, March 1998.

[11] H. Sampath, P. Stoica, and A. Paulraj, "Generalized Linear Precoder and Decoder Design for MIMO Channels Using the Weighted MMSE Criterion," *IEEE Transactions on Communications*, vol. 49, pp. 2198–2206, December 2001.

[12] D. P. Palomar, J. M. Cioffi, and M. A. Lagunas, "Joint Tx-Rx beamforming design for multicarrier MIMO channels: A unified framework for convex optimization," *IEEE Transactions on Signal Processing*, vol. 51, pp. 2381–2401, September 2003.

[13] D. J. Love and R. W. Heath, "Limited Feedback Unitary Precoding for Spatial Multiplexing Systems," *IEEE Transactions on Information theory*, vol. 51, pp. 2967–2976, August 2005.

[14] J. C. Roh and B. D. Rao, "Multiple Antenna Channels With Partial Channel State Information at the Transmitter," *IEEE Transactions on Wireless Communications*, vol. 3, pp. 677–688, March 2004.

[15] H. Lee, S. Park, and I. Lee, "Orthogonalized Spatial Multiplexing for MIMO systems," *Proc. VTC*, pp. 1–5, September 2006.

[16] H. Lee, S. Park, and I. Lee, "Orthogonalized Spatial Multiplexing for Closed-Loop MIMO systems," *IEEE Transactions on Communications*, vol. 55, pp. 1044–1052, May 2007.

[17] Y. T. Kim, S. Park, and I. Lee, "Power Allocation Algorithm for Orthogonalized Spatial Multiplexing," *Proc. Globecom*, pp. 3969–3973, November 2007.

[18] L. Collin, O. Berder, P. Rostaing, and G. Burel, "Optimal Minimum Distance-Based Precoder for MIMO Spatial Multiplexing Systems," *IEEE Transactions on Signal Processing*, vol. 52, pp. 617–627, March 2004.

[19] R. W. Heath and A. J. Paulraj, "Antenna Selection for Spatial Multiplexing Systems based on minimum error rate," *Proc. of ICC*, vol. 7, pp. 2276–2280, June 2001.

[20] H. Lee, S. Park, and I. Lee, "A New MIMO Beamforming Technique Based on Rotation Transformations," *Proc. ICC*, pp. 5359–5364, June 2007.

[21] S. H. Moon, H. Lee, Y. T. Kim, and I. Lee, "A New Efficient Group-wise Spatial Multiplexing Design for Closed-Loop MIMO Systems," *Proc. ICC*, May 2008.

Young-Tae Kim (S'07) received the B.S., M.S. degree in electrical engineering from Korea University, Seoul, Korea in 2006 and 2008, respectively, where he is currently working toward the Ph.D. degree in the school of Electrical Engineering. His research includes signal processing techniques for MIMO-OFDM systems. Mr. Kim received the silver paper award at the IEEE Seoul Section Paper Contest award in 2007.

Authorized licensed use limited to: IEEE Xplore. Downloaded on October 16, 2008 at 20:47 from IEEE Xplore. Restrictions apply.

Heunchul Lee (S'04) received the B.S., M.S., and Ph.D. degrees in electrical engineering from Korea University, Seoul, Korea, in 2003, 2005, and 2008, respectively.

During the winter of 2006, he worked as an intern at Beceem Communications, Santa Clara, CA, USA. He is currently with the Department of Electrical Engineering at Korea University, as a post-doctoral research fellow under the Brain Korea 21 Program. His research interests are in communication theory and signal processing for wireless communications, including MIMO-OFDM systems and multi-user MIMO wireless networks.

He received the Best Paper Award at the 12th Asia-Pacific conference on Communications, and the IEEE Seoul Section Student Paper Contest award, both in 2006. He was also awarded the Bronze Prize in the 2007 Samsung Humantech Paper Contest in February 2008.

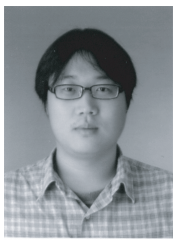

Seokhwan Park (S'05) received the B.S., M.S. degree in electrical engineering from Korea University, Seoul, Korea in 2006 and 2008, respectively, where he is currently working toward the Ph.D. degree in the School of Electrical Engineering. His research interests include signal processing techniques for MIMO-OFDM systems. Mr. Park received the Best Paper Award at the 12th Asia-Pacific Conference on Communications, and the IEEE Seoul Section Student Paper Contest award, both in 2006.

Inkyu Lee (S'92-M'95-SM'01) was born in Seoul, Korea, in 1967. He received the B.S. degree (Hon.) in control and instrumentation engineering from Seoul National University, Seoul, Korea, in 1990, and the M.S. and Ph.D. degrees in electrical engineering from Stanford University, Stanford, CA, in 1992 and 1995, respectively.

From 1991 to 1995, he was a Research Assistant at the Information Systems Laboratory, Stanford University. From 1995 to 2001, he was a Member of Technical Staff at Bell Laboratories, Lucent Technologies, where he studied the high-speed wireless system design. He later worked for Agere Systems (formerly Microelectronics Group of Lucent Technologies), Murray Hill, NJ, as a Distinguished Member of Technical Staff from 2001 to 2002. In September 2002, he joined the faculty of Korea University, Seoul, Korea, where he is currently an Associate Professor in the School of Electrical Engineering. He has published over 35 journal papers in IEEE, and has 30 U.S. patents granted or pending. His research interests include digital communications, signal processing, and coding techniques applied to wireless systems with an emphasis on MIMO-OFDM.

Dr. Lee currently serves as an Associate Editor for the IEEE Transactions on Communications and IEEE Transactions on Wireless Communications. Also, he has been a Chief Guest Editor for the IEEE Journal on Selected Areas in Communications (Special Issue on 4G Wireless Systems). He received the IT Young Engineer Award as the IEEE/IEEK joint award and the APCC Best Paper Award in 2006.

Authorized licensed use limited to: IEEE Xplore. Downloaded on October 16, 2008 at 20:47 from IEEE Xplore. Restrictions apply.